frontiers | Frontiers in Earth Science

TYPE Original Research
PUBLISHED 29 October 2024
DOI 10.3389/feart.2024.1483534

OPEN ACCESS

EDITED BY
Jan Blahůt,
Institute of Rock Structure and Mechanics (ASCR), Czechia

REVIEWED BY
Mohammad Azarafza,
University of Tabriz, Iran
Kun Fang,
Hong Kong University of Science and Technology, Hong Kong SAR, China

*CORRESPONDENCE
Xu Zongheng,
553790356@qq.com

RECEIVED 20 August 2024
ACCEPTED 23 September 2024
PUBLISHED 29 October 2024

CITATION
Xu Z, Ye H and Li L (2024) Particle size characteristics of sliding-zone soil and its role in landslide occurrence: a case study of the Lanniqing landslide in Southwest China. *Front. Earth Sci.* 12:1483534. doi: 10.3389/feart.2024.1483534

Particle size characteristics of sliding-zone soil and its role in landslide occurrence: a case study of the Lanniqing landslide in Southwest China

Zongheng Xu[1,2]*, Hongchen Ye[1,2] and Lingxu Li[3,4]

[1]Faculty of Geography, Yunnan Normal University, Kunming, China, [2]Key Laboratory of Plateau Geographic Processes and Environment Change of Yunnan Province, Kunming, Yunnan, China, [3]Department of Civil Engineering, Faculty of Engineering, Universiti Malaya, Kuala Lumpur, Malaysia, [4]School of Architecture and Engineering, Dianchi College, Yunnan University, Kunming, China

In landslide studies, particle size is a key quantitative indicator, reflecting the formation and development of the sliding zone. It plays a crucial role in understanding the mechanisms and evolutionary processes that lead to landslide occurrences. Precise measurement of particle size is crucial. This study centered on soil samples from the Lanniqing landslide in Southwest China. To begin, seven distinct methods were used to preprocess the soil samples. Next, the particle size frequency distribution was measured using the Mastersizer 2000 laser particle size analyzer. Key parameters, including median particle size, mean particle size, sorting coefficient, skewness, and kurtosis, were then compared and analyzed to determine the most appropriate preprocessing method for evaluating the characteristics of the soil samples. The mechanism of landslide occurrence was subsequently analyzed by examining the particle size characteristics, mechanical properties, and mineral composition of the soil samples. The results suggested that method C provides the most reliable analysis of particle size characteristics in soil samples. The observed coarsening of coarse particles, along with a significant increase in clay content within the sliding zone, indicates that the sliding surface has undergone multiple shear and compression events. The interplay of the upper traffic load and slope cutting at the front edge set the stage for the Lanniqing landslide, prompting the initial development of potential sliding surfaces. Rainfall acts as a catalyst for slope instability. The high clay content, combined with the formation of a low-permeability layer rich in clay minerals on the sliding surface, leads to excessive pore water pressure and mineral lubrication. These factors inherently trigger and accelerate the occurrence of the landslide.

KEYWORDS

different pretreatment, sliding-zone soil, particle size, sliding zone stagnant water, landslide occurrence

1 Introduction

The occurrence mechanisms, disaster-triggering effects and susceptibility assessment of landslides have consistently been focal points in landslide disaster research (Huang et al., 2012; Du et al., 2024; He et al., 2021; Chen et al., 2022). The former primarily centers on investigating the physical and mechanical properties of landslides through experiments or numerical simulations to uncover the mechanisms behind landslide occurrences. This research encompasses factors such as particle size, microstructure, and mineral composition, along with how these characteristics influence the permeability and the physical and mechanical properties of landslide materials. The latter focuses primarily on the movement processes and mechanisms of landslide soil deposits, as well as the stability of landslide dams. Key research areas include the movement dynamics and failure modes of landslides (Fang et al., 2024a; Pipatpongsa et al., 2014; Fang et al., 2024b). The final aspect of risk assessment primarily depends on model development and accuracy evaluation, utilizing methods such as logistic regression algorithms and machine learning (Cemiloglu et al., 2023), machine learning techniques (Yaser et al., 2023), soft computing approaches (Mao et al., 2024), and artificial neural networks (Nanehkaran et al., 2023).

A key factor in this analysis is the particle size of the sliding masses, as it directly influences the movement and deposition of these earth materials (Chen et al., 2024a). Friction and shear behavior during migration can alter the structure and particle size of landslide soil deposits. For instance, particle wear and sieving transform larger particles into smaller ones, resulting in a more uniform particle size distribution (Peng et al., 2023). This change influences the movement behavior of the soil (Peng et al., 2023; Jiang et al., 2016; Choi and Song, 2023). Additionally, particle fragmentation significantly impacts landslide dynamics, contributing to high-speed sliding (Wei et al., 2024). Finally, the characteristics of landslide soil deposits exhibit significant variability (Wang et al., 2013; Zhao et al., 2013), which in turn impacts the remaining deposit. If a landslide occurs in a mountainous area and blocks a river to form a dam, particle size influences both the velocity of the landslide as it enters the river and the cross-sectional shape of the resulting landslide dam (Zhuo et al., 2023). Additionally, particle size affects the seepage characteristics and stability of the landslide dam (Li et al., 2024; Zhou et al., 2019; Zhang et al., 2023; Shen et al., 2016; Wolter et al., 2022). The particle size of sliding masses after initiation, as well as the changes in particle size induced by external forces like friction and shear during landslide movement, is key areas of ongoing research. In fact, the particle size of the sliding-zone soil can also serve as an indicator of the landslide's development process prior to its initiation.

The formation and evolution of sliding-zone soil before landslide initiation are also crucial aspects of studying landslide mechanisms. The sliding zone, being the softest part of the landslide masses, is most likely to be the first to fail, impacting both the stability of the landslide and its deformation. During the landslide deformation process, the sliding zone undergoes extrusion, shearing, rubbing, and grinding. Notably, the heat generated by friction in the sliding zone is dissipated over the brief duration of the sliding event. The particle size will change, leading to the formation of unique and complex mineral and chemical compositions (Miao and Wang, 2022; Dong et al., 2023). The foundational aspects of geological disaster research, focusing on the engineering geological properties of sliding-zone soil, are examined in detail. The strength of sliding-zone soil is a key focus in studying landslide mechanisms, with particle size being a crucial factor. An increase in clay content within the sliding zone leads to greater shear displacement (Su et al., 2023). Additionally, a higher proportion of fine-sized particles results in lower residual strength (Zhang Y. et al., 2024). Clay particles cause seepage in sliding zones to behave differently compared to seepage in the sliding mass and sliding bed, due to variations in permeability (Wang et al., 2024). Furthermore, a calculation model that accounts for shear strength influenced by particle size can be used to predict landslide velocity and displacement (Miao and Wang, 2023). Related studies have shown significant differences in the distribution of particle size and multi-components between sliding-zone soil and the landslide itself. These differences are primarily controlled by the formation and evolution processes of the landslide (Yin et al., 2012). The more frequently the sliding-zone soil undergoes sliding, the greater the increase in fine particles (Li, 2010). Prolonged sliding typically results in a refinement of particle size in the sliding-zone soil, exhibiting distinct stage characteristics (Zhang et al., 2021). Therefore, as a quantitative analysis index in studying sliding-zone soil, particle size composition serves as an important indicator for the formation and evolution of landslides. It is crucial for analyzing the mechanisms behind landslide formation and their evolution over time.

Particle size is a key index for assessing the properties of sliding-zone soil. Common measurement methods include sieve analysis, sedimentation, light scattering, laser particle analysis, and image analysis. Particle size analysis is extensively utilized in various sediment studies, including dune sediments (Zhang H. et al., 2024), loess sediments (Zhu et al., 2024; Zhao et al., 2024), southern laterite (Wang et al., 2021; Ma et al., 2023; Sarbatly et al., 2009), and lake sediments (Deng et al., 2022; Wang et al., 2023). Among these methods, the laser particle analyzer is widely used due to its advantages of rapid analysis, high reproducibility, and excellent efficiency and accuracy. When using a laser particle size meter, the choice of pretreatment methods before measurement significantly affects the accuracy of the particle size analysis of the sample. Deng et al. (2022) and Wang et al. (2023) used the laser particle size analyzer (Mastersizer 2000, Malvern Company, United Kingdom) to ensure accurate size fractionation, though they did not specify the pretreatment methods used. The impact of different pretreatment methods on particle size test results is significant. Currently, research on the effects of pretreatment methods on the particle size analysis of sliding-zone soil is limited, and there is no consensus on the most appropriate pretreatment method for this type of soil. Therefore, the particle size characteristics of sliding-zone soil are fundamental to landslide research, making it crucial to select an appropriate pretreatment method. This paper focuses on the slip-pass slip zone soil from Qiaojia County, Zhaotong, Yunnan Province, China. Using the Mastersizer 2000 particle size analyzer and multiple particle size parameters, it examines the impact of different pretreatment methods on the particle size characteristics of the slip zone soil. The aim is to identify an appropriate pretreatment method to provide a precise data analysis basis for the material composition of the slip zone soil. Building on this, given that granularity evolution has not been extensively explored in landslide formation, the granularity

test results will be utilized to gain a deeper understanding of the underlying causes of landslides.

2 Materials and methods

2.1 Study site and sampling

The study area is situated in Qiaojia County, Zhaotong City, Yunnan Province, China. Qiaojia County borders Dongchuan County in Kunming, Huize County in Qujing, Ludian County and Zhaoyang County in Zhaotong, Yunnan Province, and is separated by the Jinsha River from Huidong County in Liangshan Prefecture, Sichuan Province (Figures 1A, B). Qiaojia is situated within the Sichuan-Yunnan meridian-directional structural system and lies at the intersection of the eastern margin of the northern section of the Sichuan-Yunnan meridian-directional structural belt and the eastern Yunnan structural region. The primary tectonic feature in the area is the Yaoshan tectonic belt. The tectonic development in the study area is primarily characterized by faults (Zhao and Xu, 2013). The area predominantly features a tectonic erosion alpine canyon landform. The Jinsha River flows from the southwest to the northwest of the county, while its tributary, the Niulan River, runs through the northeast. To the west, Yaoshan Mountain, which reaches an elevation of 4,040 m, is situated at the peak of northeast Yunnan. Xiaohe Town is situated in the northwest of the main stream of the Niulan River, nestled in a valley between two mountains, with an elevation of less than 1,000 m (Gao et al., 2011). Qiaojia features a "two rivers sandwiching a mountain" landform, characterized by significant elevation differences and pronounced terrain relief. Xiaohe Town is one of the 17 towns in Qiaojia County and is situated in the northeastern part of the county. The highest point in Xiaohe Town is Mantianxing in Shanbao Village, with an altitude of 3,300 m. Xiaohe is located at the intersection of Lufang Valley and Yinchang Valley, which are part of the Niulan River system—a tributary of the Jinsha River that originates in Songming County, Kunming City. Due to intense erosion by the Niulan River, combined with the effects of fractures and folds, geological disasters frequently occur in Xiaohe Town, resulting in significant economic losses and casualties. The sampling location for this paper is Lanniqing Village, an administrative village within Xiaohe Town. At approximately 4:40 a.m. on 5 September 2019, the northeast slope of Lanniqing Village experienced a landslide due to continuous heavy rainfall and the long-term impact of driving loads on the Shan-ma line road at the trailing edge. Approximately 20,000 cubic meters of fractured mudstone mixed with gray, purple clay, and sub-clay rapidly slid down the slope. The significant height difference exacerbated the situation, leading to a geological disaster that resulted in nine people being buried, two families affected, and substantial destruction of houses, causing significant casualties and economic losses (Figure 1C) (Chen et al., 2024b).

Through a field study of the Lanniqing landslide and analysis of remote sensing images, we determined that the sliding source area of the landslide is approximately 2,000 square meters (Figure 2A). The transport-scraping area measures about 2,500 square meters (Figure 2B), while the deposit and disaster-causing area totals around 5,000 square meters. The sliding-zone soils from the source area, primarily surrounded by the Shan-ma line, the access route to Lanniqing Village, and its left and right boundaries, was studied to assess the impact of different pretreatment methods on the particle size. This involved identifying a suitable pretreatment method and analyzing how particle size affects the mechanical properties of the soil, as well as the role of sliding-zone soil in landslide occurrence. Sampling was conducted in the sliding source area (Figures 1C, 2A). We selected an area with minimal anthropogenic disturbance, removed surface piles and debris formed by rainfall runoff erosion, and collected approximately 2 kg of soil from the smooth surface of the sliding zone in two locations, labeled QJ1-1 and QJ2-1. Additionally, undisturbed subsoil samples from a depth of 100 cm were collected for comparative analysis, labeled QJ1-5 and QJ2-5. These samples were used to determine particle size characteristics. For soil shear strength determination, samples were also taken using 30 cm^2 × 2 cm ring cutters at the same locations (Figures 2C–F).

2.2 Testing process

To investigate the impact of various pretreatment methods on both sliding-zone soil and undisturbed subsoil, the samples were air-dried and then sieved through a 2 mm mesh. Seven sets of experiments will be conducted for each soil sample, corresponding to seven pretreatment methods (denoted as A, B, C, D, E, F, and G). In total, 28 samples will be tested. To minimize measurement errors, each sample will undergo three repetitions for each experiment, and the final results will be averaged for analysis. Each soil sample tested weighed 0.2 g. The particle size analysis was conducted using the Mastersizer 2000 (M2000), which has a range of 0.02–2000 μm. The Mastersizer 2000 (M2000) features 52 detectors on a single lens, enabling it to measure a wide particle size range from 0.02 to 2000 μm without the need for initial sample fractionation (Callesen et al., 2018). The M2000 uses laser diffraction to measure particle size. The process begins with monochromatic light emitted from a laser, which is expanded into parallel light through a filtering device and directed onto the particles, creating a diffraction pattern. The diffracted light passes through a Fourier lens, focusing the scattered light in the same direction to form a diffraction ring. The intensity distribution of the scattered light is related to the size and quantity of the particles. This scattered light is focused onto detectors, which measure its angular distribution. The light intensity signal is then converted into an electrical signal, which is amplified and used to calculate the equivalent particle size (Ramaswamy and Rao, 2006; Jiang et al., 2015). The different pretreatment methods were applied as follows (Zha et al., 2022):

A: The soil samples were saturated with purified water and left in a beaker for 24 h before being tested without additional treatment.

B: The soil samples were saturated with purified water and left in a beaker for 24 h. They were then treated with 10 mL of 0.05 mol/L $(NaPO_3)_6$, followed by 10 min of agitation in an ultrasonic cleaner before measurement.

C: The soil samples were treated with 10 mL of 10% H_2O_2 and boiled on a heating plate until no bubbles were observed. After removing the solution, 10 mL of 0.05 mol/L $(NaPO_3)_6$ was added. The mixture was then agitated in an ultrasonic cleaner for 10 min before measurement.

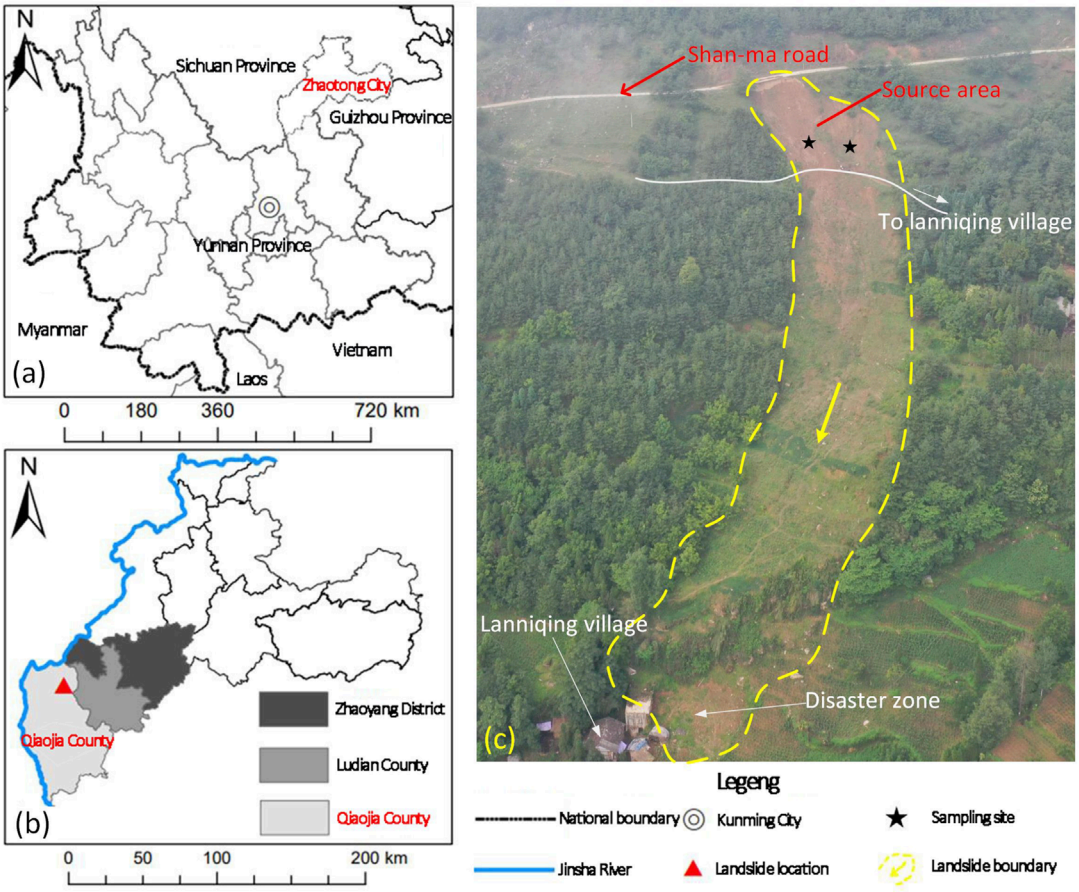

FIGURE 1
Landslide location and sampling setup overview: **(A,B)** Landslide location in Yunnan Province and Zhaotong City. **(C)** Overview of the landslide and the sampling sites.

D: The soil samples were treated with 10 mL of 10% HCl and then saturated with purified water in a beaker for 24 h. After removing the water, 10 mL of 0.05 mol/L $(NaPO_3)_6$ was added. The mixture was then agitated in an ultrasonic cleaner for 10 min before measurement.

E: The soil samples were first treated with 10 mL of 10% H_2O_2 and boiled on a heating plate until no bubbles were observed. They were then treated with 10 mL of 10% HCl and saturated with purified water in a beaker for 24 h. After removing the water, 10 mL of 0.05 mol/L $(NaPO_3)_6$ was added. The mixture was then agitated in an ultrasonic cleaner for 10 min before measurement.

F: The soil samples were saturated with purified water and left in a beaker for 24 h. They were then agitated in an ultrasonic cleaner for 10 min before measurement.

G: The soil samples were treated with 10 mL of 10% HCl and then saturated with purified water in a beaker for 24 h.

In the pretreatment methods described, hydrochloric acid (HCl) is primarily used to remove the effects of carbonate cementation, while hydrogen peroxide (H_2O_2) is employed to eliminate the influence of organic matter agglomeration. Additionally, sodium hexametaphosphate ($(NaPO_3)_6$) is used to address issues related to particle dispersion. The results from various pretreatment methods were compared to assess the impact of different treatments and reagents on particle size characteristics. For instance, methods A and F were compared to evaluate the effect of oscillation, while methods B and F were used to determine the influence of $(NaPO_3)_6$. The comparison between methods A and G examined the effect of HCl in the presence of other reagents, and the comparison of methods C and E highlighted the effect of HCl when used with H_2O_2 and $(NaPO_3)_6$. It is necessary to note that mineral composition analysis was performed using X-ray diffraction (XRD), microstructural observations were made with a Scanning Electron Microscope (SEM), and shear testing was conducted using a direct shear test apparatus.

2.3 Computational method

Here, the widely used graphical method (Folk and Ward, 1957) was employed to calculate, compare, and analyze the particle size test results of different pretreatment methods. This method is commonly utilized for grain size analysis of sediments. This method is preferred for its speed and accuracy, effectively minimizing

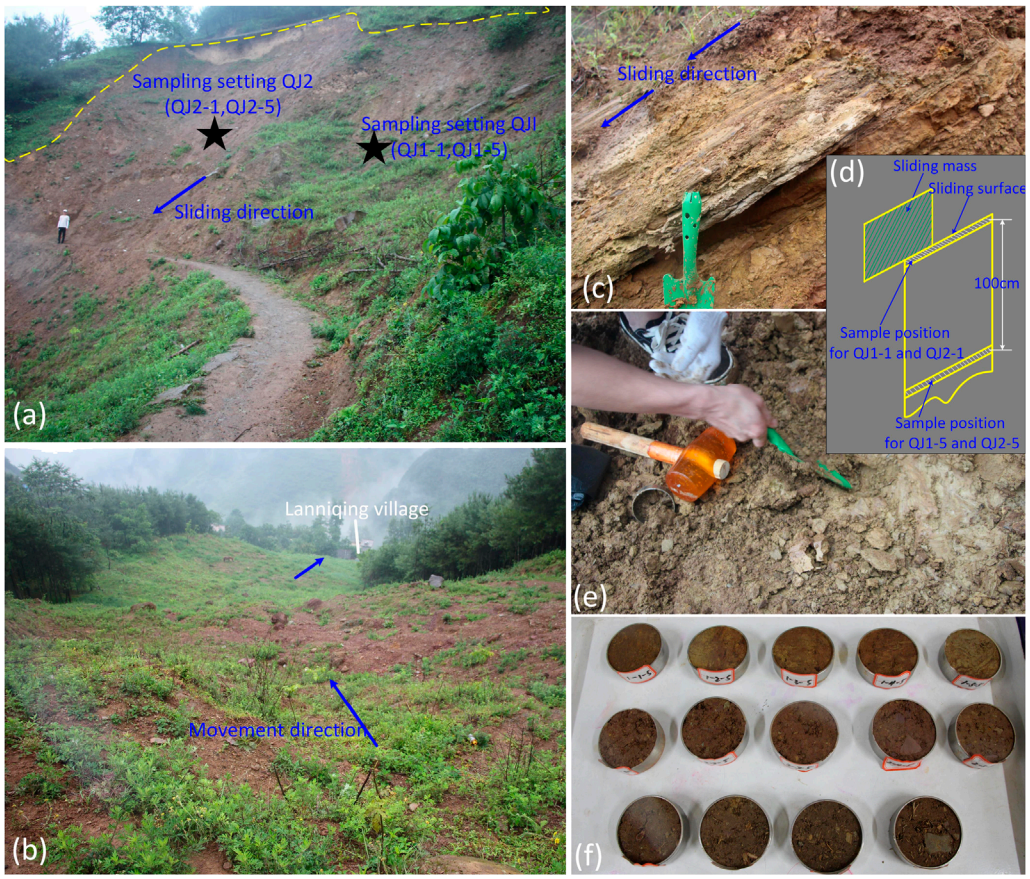

FIGURE 2
Overview of the sliding source area and soil sampling locations: **(A,B)** Sliding source area showing sampling sites and landslide flow zone. **(C-E)** Photographs and schematic illustrations of the sampling. **(F)** Soil samples prepared for laboratory testing.

the impact of outliers on the data. It is particularly useful for comparing grain size data across different processing results and can also be applied to study the particle size of sliding-zone soil. The parameters commonly used to describe the statistical characteristics of particle size in this method include: median particle size (Md), mean particle size (Mz), sorting coefficient (Sd), skewness (Sk) and kurtosis (Ku). These parameters offer various perspectives on particle size characteristics. The particle size distribution can be analyzed through the median and mean particle sizes, which reflect the central tendency of particle size. The sorting coefficient indicates the uniformity of the particle size distribution. Skewness measures the asymmetry of the particle size distribution, while kurtosis assesses the sharpness of the particle frequency curve. The cumulative curve (Figures 3B, D, F, H) was derived from the frequency distribution of particle size measurements (Figures 3A, C, E, G) obtained using the M2000. By selecting values from representative points and applying the calculation equations listed in Table 1, the parameters were quantified. In the table, the ϕ values are calculated using the Krumbein transform method: $\phi = -\mathrm{Log}_2(D)$, where D represents the particle size in millimeters (mm). The values ϕ_5, ϕ_{16}, ϕ_{25}, ϕ_{50}, ϕ_{75}, ϕ_{84}, and ϕ_{95}– represent the particle sizes corresponding to 5%, 16%, 25%, 50%, 75%, 84%, and 95% on the cumulative curves, respectively.

3 Results and discussion

3.1 Characteristics of particle size distribution

Figure 3 displays the particle size frequency distribution curves for the sliding-zone soil samples QJ1-1 and QJ2-1, as well as the undisturbed subsoil samples QJ1-5 and QJ2-5. It is evident that the frequency distribution curves for the same sample vary significantly depending on the pretreatment method used. Firstly, the analysis of sample QJ1-1 revealed that the frequency curve for QJ1-1A, which underwent only purification with water, exhibited a single-peak shape. The peak particle size was approximately −1.6ϕ, indicating a coarse particle size. The oscillatory process using an ultrasonic cleaner (QJ1-1F) resulted in noticeable changes, producing a multi-peak morphology. The highest peak occurred around −0.46ϕ, and the overall curve shifted to the right, indicating that the particle size became finer. With the addition of $(NaPO_3)_6$ (QJ1-1B), the curve transitioned to a single-peak morphology. The peak particle size remained at −0.46ϕ, but the percentage increased from 3.42% to 4.42%, indicating a noticeable rise in the proportion of fine particles. The above analysis indicates that both the oscillatory process and the addition of $(NaPO_3)_6$ had a substantial dispersing effect on the particles, leading to a notably finer particle size. Additionally, the

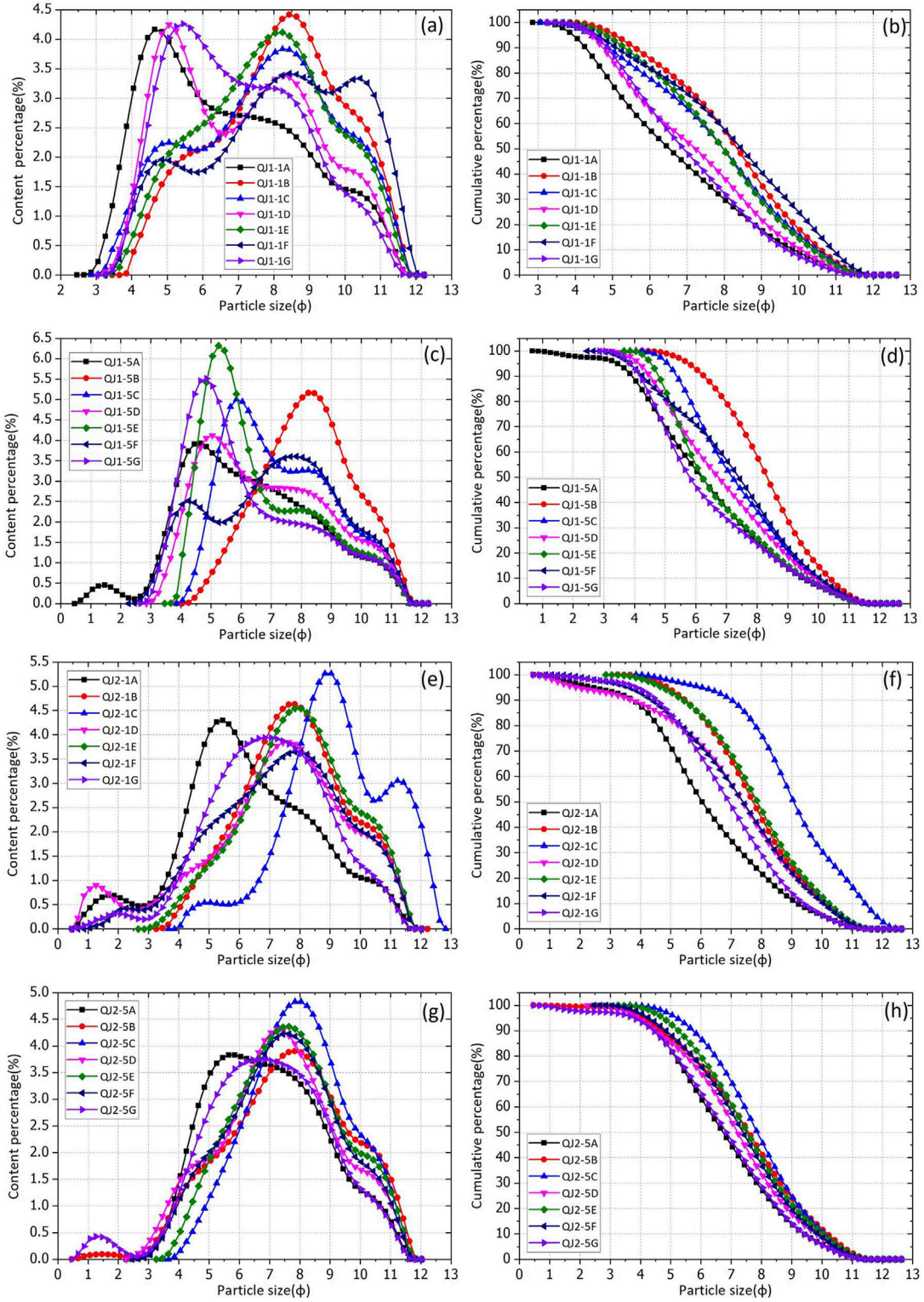

FIGURE 3
The particle size frequency distribution and cumulative curves for sliding-zone soil subjected to various pretreatment methods. In the legend, QJ1-1 and QJ1-5 represent samples from QJ1, while QJ2-1 and QJ2-5 are from QJ2. **(A–H)**: different pretreatment methods used for particle size testing.

TABLE 1 Computational feature parameters by graphic method.

Parameters	Calculation equations
Median particle size (M_d)	$M_d = \phi_{50}$
Mean particle size (M_z)	$M_z = \frac{1}{3}(\phi_{16} + \phi_{84} + \phi_{50})$
Sorting coefficient (S_d)	$S_d = \frac{\phi_{84}-\phi_{16}}{4} + \frac{\phi_{95}-\phi_5}{6.6}$
Skewness (S_k)	$S_k = \frac{1}{2}\left(\frac{\phi_{84}+\phi_{16}-2\phi_{50}}{\phi_{84}-\phi_{16}} + \frac{\phi_{95}+\phi_5-2\phi_{50}}{\phi_{95}-\phi_5}\right)$
Kurtosis (K_u)	$S_u = \frac{\phi_{95}-\phi_5}{2.44(\phi_{75}-\phi_{25})}$

analysis of the effect of HCl on particle size showed that the curve for soil sample QJ1-1G, treated with HCl, was similar to that of QJ1-1A, with only a slight shift to the right. The peak particle size changed from −1.6 ϕ to −1.36 ϕ, suggesting a slight tendency toward coarser particle size after the addition of HCl, though the change was not pronounced. Comparing QJ1-1B and QJ1-1D shows that, despite the particles being well-dispersed due to the oscillatory process and $(NaPO_3)_6$, the addition of HCl induces significant changes in particle size. The curve for QJ1-1D shifts to the left, with the peak particle size changing from −0.46 ϕ to −1.48 ϕ. The morphology of the curve transitions from single-peak to multi-peak, indicating a noticeable coarsening of the particle size. This is because, when particles are finely dispersed, incomplete removal and cleaning with HCl can lead to the cohesion of clay particles, significantly reducing the content of fine particles. Additionally, during the removal and cleaning process with HCl, some finer particles may be lost. As a result, these factors contribute to the observed coarsening of the particle size. The results from QJ1-1G reveal that the coarsening effect of particle size caused by HCl is more pronounced compared to other methods. Comparing QJ1-1B and QJ1-1C shows that after adding H_2O_2, $(NaPO_3)_6$, and using the oscillatory process, the peak particle size remains at −0.46ϕ, and the curve shape is consistent. The addition of H_2O_2 resulted in only a slight increase in the content of fine particles, with the most notable change being a reduction in peak content from 4.42% to 3.83%, representing a decrease of −0.59%. Therefore, the impact of H_2O_2 on particle size in the pretreatment of sliding-zone soils with minimal organic matter is negligible. Additionally, it was found that the traditional E method for particle size testing pretreatment is not the most suitable approach.

In Figures 3E–H, the particle size curves for QJ2-1 show noticeable differences due to various pretreatment methods, with the particle sizes generally being coarse. For sample QJ2-1A, the peak particle size remains large, approximately −1.36ϕ, which is similar to the value observed in QJ1-1A. The curve for QJ1-1F shifts to the right overall, indicating a significant reduction in particle size. In contrast, the curve for QJ2-1F, processed using the same method, exhibits a pronounced multi-peak morphology. The peak particle size for QJ2-1F is about −0.46ϕ, with a percentage of 3.65%, which is comparable to that of QJ1-1F. The peak particle size of the QJ2-1B curve is also at −0.64ϕ, but it shows an increase in fine-grained particles. In contrast, the QJ2-1C curve, which was treated with H_2O_2, differs significantly from QJ1-1. It shifts to the right and displays a multi-peak morphology, with a peak particle size of −0.34ϕ and a percentage of 5.26%. The particle size of QJ2-1 is notably finer, likely because QJ2-1 was sampled from a slope where organic matter, carried by surface water, accumulates, resulting in a higher organic matter content compared to QJ1-1. The addition of H_2O_2, which removes organic matter, had a significant impact on the particle size results for QJ2-1. In other respects, the effects of different pretreatment methods on the particle size results for QJ2-1 are similar to those observed for QJ1-1, and thus will not be further discussed.

3.2 Particle size parameters

Further research is needed to quantitatively analyze the impacts of different pretreatment methods on particle size parameters. Following the particle size grading standards (Shaanxi North team of Chengdu University of Geology, 1978), soil samples are categorized into clay (<2 μm), silt (2–63 μm), and sand (>63 μm), and the percentage for each size interval is calculated (Figure 4). The particle size parameters for each soil sample were then computed using the graphical method, as detailed in Table 2. The impact of different pretreatment methods on the percentage of each particle size interval is also significant. For QJ1-1, the particles are primarily silt, followed by clay, with sand being the least prevalent. After adding purified water (QJ1-1A), the sample showed a lower clay content (17.46%) and a higher silt content (76.09%), with median and mean particle sizes of 6.33ϕ and 6.56ϕ, respectively. In contrast, QJ1-1G, treated with HCl, exhibited a decrease in clay content (16.74%) and an increase in sand content (82.09%), with median and mean particle sizes of 6.70ϕ and 6.86ϕ, respectively, indicating a coarsening of particle size. QJ1-1F, which underwent ultrasonic treatment, demonstrated a significant increase in clay content (40.31%) and a decrease in silt (58.60%), with median and mean particle sizes of 8.27ϕ and 8.06ϕ, respectively. This sample had the finest particle size among all pretreatment methods. Compared to QJ1-1F, the particle size interval percentages, median particle size (8.15ϕ), and mean particle size (8.03ϕ) of QJ1-1B were smaller, indicating that $(NaPO_3)_6$ had a dispersing effect on the particles. However, this effect was less pronounced than that achieved through ultrasonic oscillation. QJ1-1D, which was treated with HCl, showed a low clay content (21.57%) and median and mean particle sizes of 7.03ϕ and 7.05ϕ, respectively. This indicates that HCl significantly coarsened the particle size compared to samples treated with other chemical reagents. The HCl tends to increase the grain size, a phenomenon supported by existing literature. On one hand, the removal and cleaning effects of HCl can lead to the loss of finer particles, particularly when other chemical reagents are involved (Wang et al., 2018). Additionally, excess HCl can react with clay minerals (such as chlorite and kaolinite), causing particle coagulation and resulting in further coarsening of the particle size (Liu et al., 2012). In contrast, QJ2-1C, treated with H_2O_2, had the highest clay content (56.05%), with silt at 43.95% and no sand, resulting in a median particle size of 9.07φ. This suggests that the dispersing effect of H_2O_2 was more pronounced compared to the effect of $(NaPO_3)_6$, as seen in QJ2-1B.

Based on the above analysis of particle size curves and parameters, it is clear that both ultrasonic oscillation and $(NaPO_3)_6$ effectively dispersed the particles during pretreatment. However, the dispersing effect of ultrasonic oscillation was more pronounced than that of $(NaPO_3)_6$. The use of HCl resulted in a reduction of

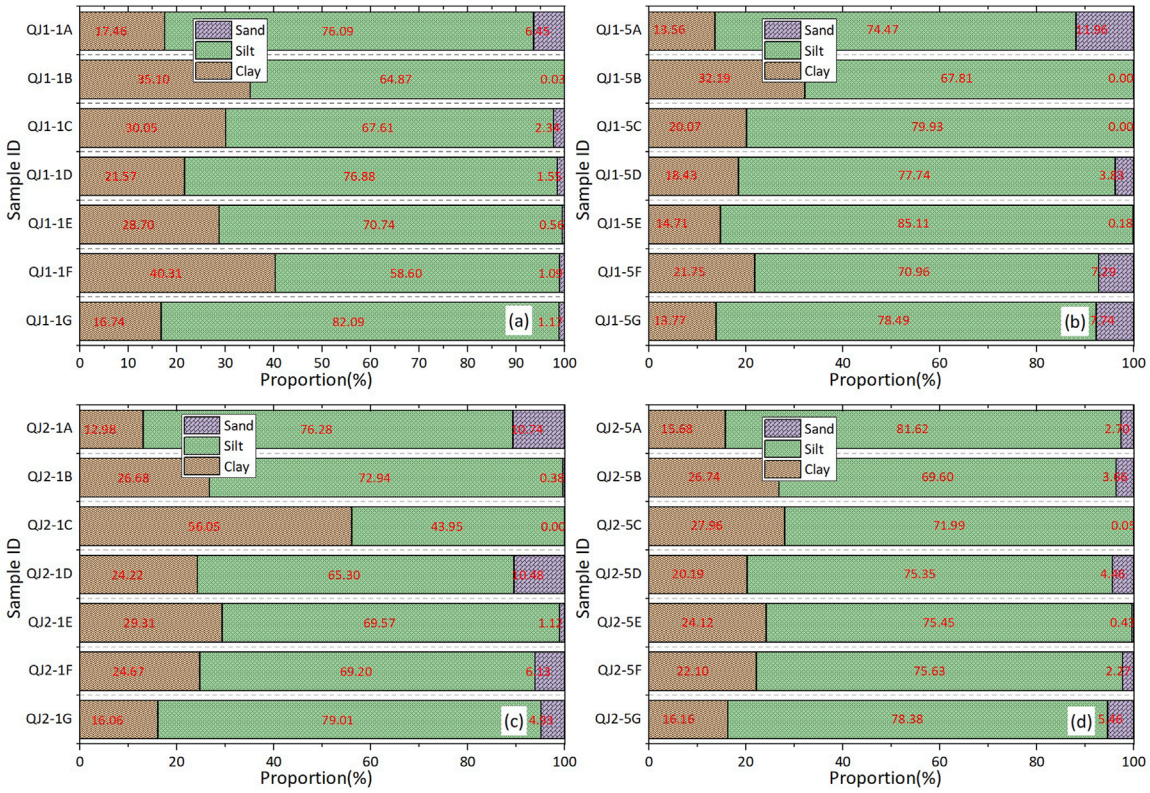

FIGURE 4
Interval proportion of particle content in soil samples: **(A)** QJ1-1 with different pretreatment methods. **(B)** QJ1-5 with different pretreatment methods. **(C)** QJ2-1 with different pretreatment methods. **(D)** QJ2-5 with different pretreatment methods.

TABLE 2 Particle size parameters of soil samples calculated by graphic method.

Samples ID	M_d	M_z	S_d	S_k	K_u	Samples ID	Md	Mz	Sd	Sk	Ku
QJ1-1A	6.33	6.56	2.15	0.19	0.80	QJ1-5A	5.99	6.22	2.16	0.18	0.87
QJ1-1B	8.15	8.03	1.90	−0.10	0.93	QJ1-5B	8.13	8.12	1.57	−0.01	0.97
QJ1-1C	7.78	7.60	2.13	−0.10	0.87	QJ1-5C	6.99	7.20	1.75	0.20	0.83
QJ1-1D	7.03	7.05	2.05	0.05	0.76	QJ1-5D	6.54	6.74	2.07	0.17	0.81
QJ1-1E	7.77	7.70	1.93	−0.05	0.91	QJ1-5E	6.01	6.51	1.85	0.41	0.86
QJ1-1F	8.27	8.06	2.21	−0.14	0.84	QJ1-5F	7.20	7.01	2.21	−0.09	0.87
QJ1-1G	6.70	6.86	1.86	0.15	0.83	QJ1-5G	5.60	6.14	2.07	0.39	0.87
QJ2-1A	6.05	6.69	2.17	0.13	0.81	QJ2-5A	6.73	6.82	1.88	0.10	0.89
QJ2-1B	7.73	7.86	1.76	0.01	0.91	QJ2-5B	7.58	7.52	2.07	−0.05	0.96
QJ2-1C	9.07	7.99	1.73	−0.06	1.02	QJ2-5C	7.86	7.89	1.66	0.02	0.98
QJ2-1D	7.38	7.23	2.14	−0.05	0.90	QJ2-5D	7.21	7.18	1.99	−0.02	1.02
QJ2-1E	7.86	7.40	2.23	−0.04	0.86	QJ2-5E	7.52	7.56	1.81	0.04	0.96
QJ2-1F	7.40	7.39	2.31	−0.05	0.78	QJ2-5F	7.39	7.36	1.91	−0.02	0.98
QJ1-1G	6.92	6.95	2.08	−0.02	0.89	QJ1-5G	6.84	6.86	1.94	0.02	0.94

clay content, an increase in silt, and a general coarsening of the particle size. For sliding-zone soil with a high clay content, these changes can lead to biased particle size test results. Therefore, it is advisable not to use HCl in the particle size measurement of sliding-zone soil. Given that the organic matter in the sliding-zone soil is generally low, the impact of H_2O_2 during pretreatment is minimal. Therefore, this paper recommends discussing the particle size results obtained using pretreatment method C for analyzing landslide occurrences.

3.3 Physical and mechanical characteristics of sliding zone soil

3.3.1 Characteristic of particle size

The particle size of sliding-zone soil is fundamental for understanding the engineering geological properties associated with landslides. After pretreatment using method C, the frequency distribution curves for sliding-zone soils QJ1-1 and QJ2-1 exhibit a multi-peak morphology, in contrast to the single-peak morphology observed for undisturbed subsoil samples. For QJ1-1, the particle size distribution percentages are 2.34% sand, 67.61% silt, and 30.05% clay. For QJ2-1, the percentages are 0% sand, 56.05% silt, and 43.95% clay. In comparison, the undisturbed subsoil samples show different distributions: QJ1-5 has 0% sand, 79.93% silt, and 20.07% clay, while QJ2-5 has 0.05% sand, 71.99% silt, and 27.96% clay. In terms of particle size parameters, the median and mean particle sizes, along with the sorting coefficients, differ between the sliding-zone soils and the undisturbed subsoil. For QJ1-1, the median particle size is 7.78 ϕ, the mean particle size is 7.60 ϕ, and the sorting coefficient is 2.13. For QJ2-1, these values are 9.07 ϕ for the median, 7.99 ϕ for the mean, and 1.73 for the sorting coefficient. In comparison, the undisturbed subsoil samples show median and mean particle sizes of 6.99 ϕ and 7.20 ϕ with a sorting coefficient of 1.75 for QJ1-5, and 7.86 ϕ and 7.89 ϕ with a sorting coefficient of 1.66 for QJ2-5. These results indicate that the particle size distribution of sliding-zone soils is notably finer than that of the undisturbed subsoil, as evidenced by both the frequency distribution curves and particle size parameters. During the landslide process, the sliding-zone soil undergoes shear, extrusion, and abrasion, leading to a reduction in coarse particles and an increase in fine particles. This results in a shift from a single-peak to a multi-peak morphology in the particle size distribution curve, with an additional peak appearing in the fine-grained interval. In terms of percentage distribution, the sliding-zone soils are primarily composed of silt, followed by clay, with sand present in smaller amounts. In contrast, the undisturbed subsoils have a significantly higher clay content—an increase of 10%–20%—at the expense of silt and sand. The median and mean particle sizes of the sliding-zone soil are smaller and finer compared to those of the undisturbed subsoils, though the differences between them are not substantial. The observed fining and notable increase in clay content in the sliding-zone soil, resulting from external forces during the sliding process, resemble the particle size characteristics seen in the landslide of the accumulated massive loose layer in Tangjiashan, Yunnan Province, China (Chen et al., 2015). Through site investigation and remote sensing image analysis of the Lanniqing landslide, it was observed that prior to the landslide, the front edge of the slope had been affected by engineering cutting due to road construction leading to Lanniqing Village. Additionally, long-term traffic load from the Shan-ma road at the back edge of the slope had induced creep deformation. Significant deformation has occurred, with a more pronounced depression zone forming at the back edge. At this stage, a potential sliding surface has developed, and creeping sliding has begun. During the landslide's incubation and the evolution of the sliding zone, the soil has experienced multiple stages of varying degrees of shear sliding and extrusion. Combined with groundwater activity, this has led to a gradual increase in fine particles within the sliding zone.

3.3.2 Mechanical characterization and relationship to its particle size

The particle size of the sliding-zone soil reflects the evolutionary process of landslide movement and significantly impacts the soil's mechanical properties, which in turn influences landslide occurrence and development. Since soil mechanical characteristics, which are affected by particle size composition, are crucial for determining landslide stability, research into these characteristics is essential. Direct shear tests were performed to investigate these properties, and the stress-strain curves for the soil samples are presented in Figure 5. Under consistent vertical pressure, shear stress in the soil samples increases with shear displacement, though the rate of increase slows down over time until the soil fails due to shear. The shear deformation characteristics of the soil samples are generally similar. However, a few samples, such as QJ1-1 (at 300 kPa) and QJ2-1 (at 100 kPa), exhibit properties akin to dense clay, showing a distinct peak value and strain-softening behavior. These peak values can be used to determine the shear strength of the samples. In contrast, most samples display no distinct peak value and instead show strain-hardening behavior. After reaching a certain degree of shear deformation, the shear stress continues to increase until the shear surface is fully ruptured due to the stick-slip effect characteristic of "soft clay" on the shear surface. Additionally, some soil samples show minimal variation in shear strength across different vertical pressures, suggesting that changes in vertical pressure have a limited impact on shear strength. These observations highlight the unique properties of the sliding-zone soil from the Lanniqing landslide.

Based on the shear strength measurements from the soil samples and Coulomb's law, the values of shear strength, cohesion c, and internal friction angle ϕ for each soil sample are summarized in Table 3. It is observed that the shear strength of the soil increases with the increase in vertical pressure. The shear strength of most sliding-zone soils is higher compared to that of the undisturbed subsoils. Notably, the shear strength of QJ2-1 and QJ2-5 is greater than that of QJ1-1 and QJ1-5. The comparison of shear strength indicators reveals the following: for QJ1-1 and QJ1-5, the cohesion values are 33.02 kPa and 5.44 kPa, while the internal friction angles are 15.11° and 21.08°, respectively. For QJ2-1 and QJ2-5, the cohesion values are 119.34 kPa and 11.94 kPa, with internal friction angles of 15.11° and 24.23°, respectively. So the cohesion of the sliding-zone soils is significantly higher compared to the undisturbed subsoils, whereas the internal friction angles of the sliding-zone soils are generally lower. The determinants of shear strength indicators reveal that cohesion arises from factors like cementation and electrostatic molecular attraction between soil

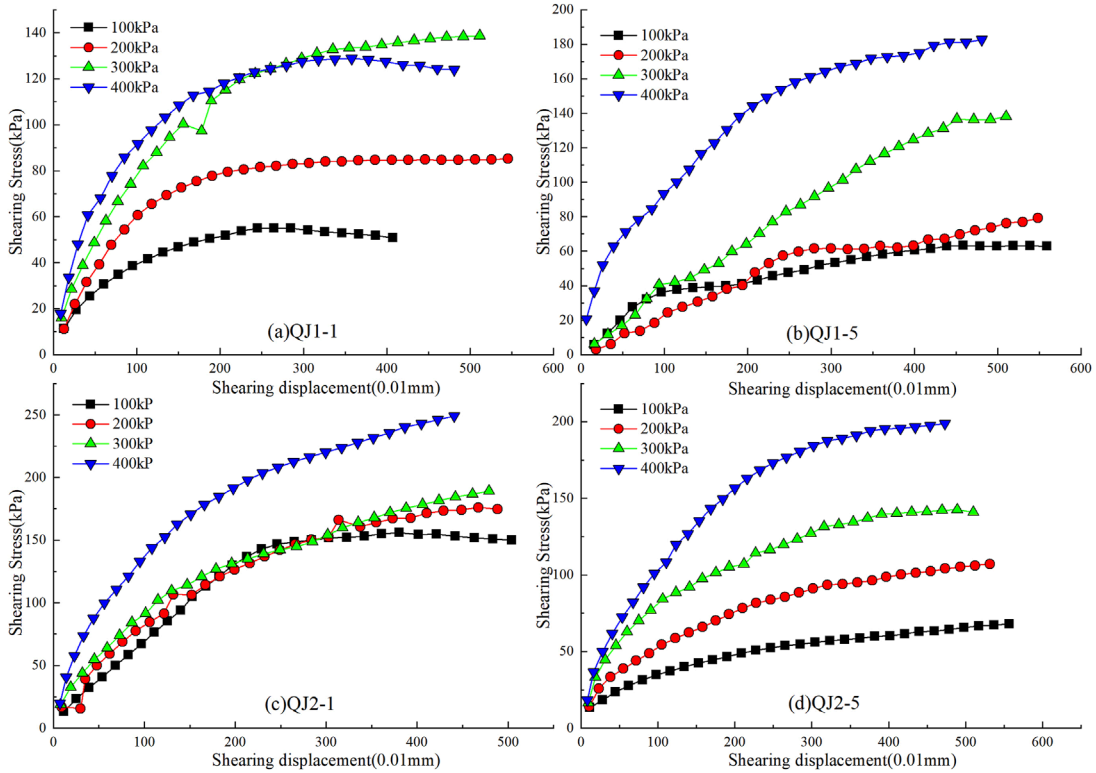

FIGURE 5
Stress-strain curves from shear tests of soil samples: **(A)** QJ1-1 under different vertical pressure. **(B)** QJ1-5 under different vertical pressure. **(C)** QJ2-1 under different vertical pressure. **(D)** QJ2-5 under different vertical pressure.

TABLE 3 The shear strength and its indicators of each soil sample.

Vertical pressure/kPa		100	200	300	400	c/kPa	ϕ/°
Sample ID	QJ 1-1	55.09	84.66	134.50	128.80	33.02	15.16
	QJ 1-5	60.50	64.08	124.80	174.20	5.44	21.89
	QJ 2-1	155.87	169.13	177.37	242.19	119.34	14.96
	QJ 2-5	60.22	98.84	139.83	195.39	11.95	24.06

particles, and it is influenced by the presence of fine grains and moisture content. In contrast, the internal friction angle is derived from the surface roughness friction between soil particles along the shear plane and the interlocking force generated by particle interembedding. This angle is affected by vertical stress, particle size distribution, and the shape of the particles. Based on the particle size test results, it was observed that the slip-belt soils QJ1-1 and QJ2-1 contain significantly higher clay content, with smaller median and mean particle sizes. This suggests that the variations in shear strength and its indicators among the soil samples are attributable to differences in particle size. The high fine particle content in the sliding zone is likely due to the sliding surface undergoing multiple stages of displacement and sliding, which contributes to the distinct shear strength characteristics of these soils.

The X-ray diffraction analysis of the sliding-zone soils, as shown in Figure 6, reveals that these soils are primarily composed of chlorite, mica, quartz, and potash feldspar. Specifically, chlorite content ranges from 10% to 15% in some samples and 5%–10% in others, while mica content ranges from 20%–25% to 15%–20%. Quartz is the most abundant mineral, comprising 50%–60% in some samples and 60%–70% in others, while potash feldspar content varies between 5% and 10%. The substantial presence of chlorite and mica, which together make up nearly 40% of the composition, is particularly noteworthy. These minerals, along with the weathering products of mica (such as hydrated mica and illite), are classified as layered aluminosilicates and exhibit high sensitivity to water. This sensitivity significantly influences the unique properties of the sliding-zone soil.

4 Discuss on landslide occurrence

Accurate measurement of particle size is fundamental to studying the characteristics of the sliding zone. The evolution of the sliding zone, marked by changes in particle size and mechanical strength, reveals that it undergoes disturbances at multiple stages during the occurrence and development of a landslide. In this context, it is essential to examine the failure mechanism of rain-induced landslides based on precise particle size measurements of sliding-zone soils.

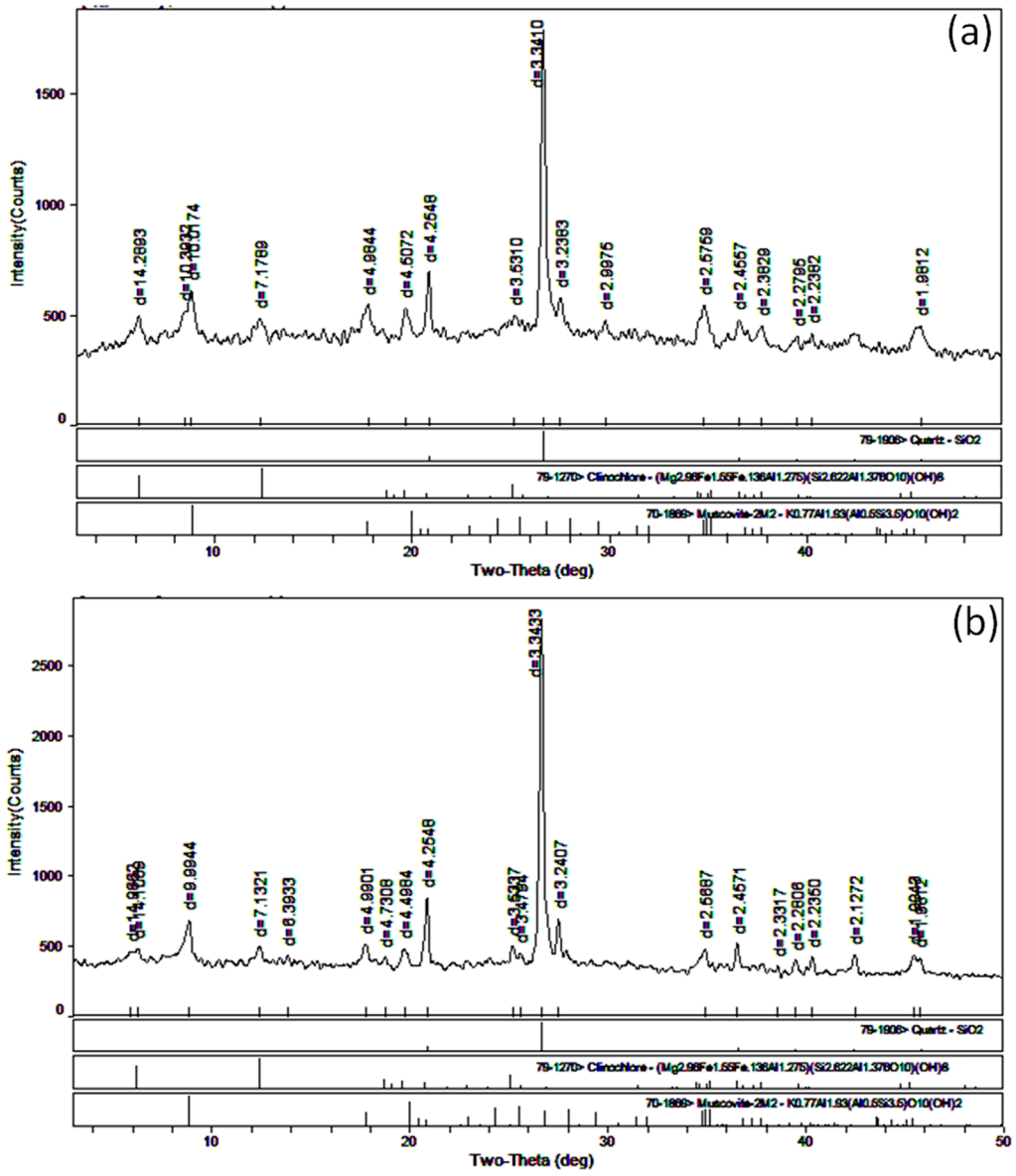

FIGURE 6
X-ray diffraction pattern of sliding-zone soils of Lanniqing landslide: **(A)** QJ1-1. **(B)** QJ2-1.

Based on the site investigation, the Lanniqing landslide is identified as a shallow landslide, with a shallow sliding surface (Figure 2A). Extensive and detailed research has been conducted by scholars on the failure mechanisms of rainfall-induced shallow landslides. The prevailing understanding is that the rapid infiltration of rainfall causes the landslide mass to gradually become saturated, resulting in a decrease in matric suction and an increase in pore water pressure. The primary cause of shallow landslides is the reduction in effective stress and soil shear strength (Gidday et al., 2023; Bai et al., 2022; Zhang et al., 2021). For example, in the central mountainous region of Ethiopia, a shallow landslide was triggered by the formation of a potential sliding surface within a low-permeability layer, leading to a rise in the transient groundwater level, decreased suction, and reduced shear strength, ultimately resulting in slope failure (Gidday et al., 2023). The vertical infiltration of heavy rainfall, induced by a typhoon in Fujian Province, China, along with changes in the seepage environment due to groundwater migration, are key factors contributing to the shallow sliding failure of granite residual slopes (Bai et al., 2022). A similar mechanism can also explain the shallow instability observed in water-sensitive loess (Zhang et al., 2021). In conclusion, applying the upper stagnating water theory is a reasonable approach to explaining the mechanism behind landslides in areas rich in clay particles within the sliding zone. Additionally, rainfall infiltration increases permeability, which elevates the sliding force, while the migration and local accumulation of fine particles during seepage play a crucial role in triggering shallow landslides. Therefore, the Lanniqing landslide results not only

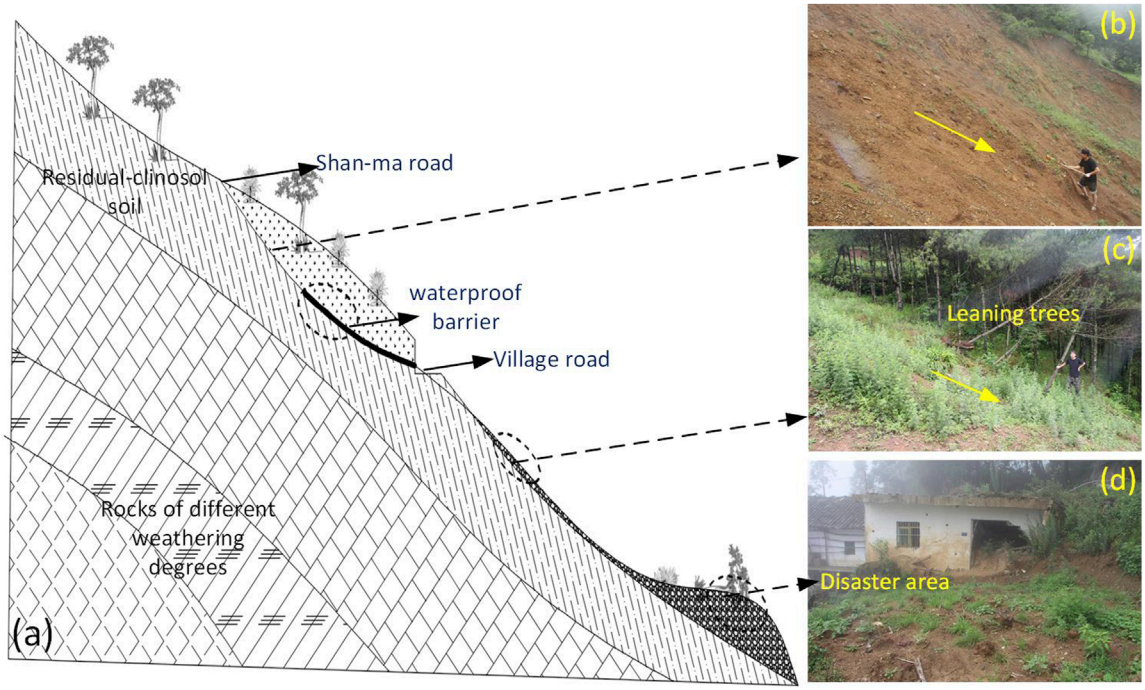

FIGURE 7
Overview of the Lanniqing landslide: **(A)** Generalized model of Lanniqing landslide occurrence. **(B-D)** Site survey images of each zone of the landslide.

from water stagnation in the upper layers, particularly within the sliding zone, but also from changes in soil structure due to the sliding process.

Initially, the occurrence of the landslide is examined using the upper stagnating water theory for shallow landslides. According to this theory, rainfall leads to the accumulation of pore water pressure in the sliding zone, promoting landslides. This excess pore water pressure is directly linked to the grain size characteristics of the sliding zone soil and is influenced by the rapid infiltration and accumulation of water. The high-viscosity sliding zone, resulting from multi-stage shear dislocation, forms the foundation for this analysis. The source area of the landslide in Lanniqing village is located in the middle to rear part of the slope, where there is a significant change in terrain elevation. Over time, the stress on the slope increased due to prolonged vehicle loads from the Shan-ma road. Despite this, the slope did not show significant deformation under the vehicle load. To enhance access, local villagers constructed a road in the lower part of the sliding source area, resulting in a vertical cut approximately 5 m high, but without any protective measures like retaining walls or drainage systems. Meanwhile, vehicle loads from the Shan-ma road continued to apply pressure on the slope. The combined impact of these factors led to the formation of tension cracks and a noticeable depression zone at the trailing edge, making the edge cutting slope a critical factor in the development of the sliding zone. The multi-stage sliding along the surface results in an accumulation of fine-grained soil in the sliding zone, which contributes to the formation of a local waterproof barrier (Figure 7). Additionally, microstructural observations indicate that the sliding-zone soil contains a high proportion of schistose aggregated minerals (Figure 8), predominantly aluminum silicate minerals such as mica and chlorite, as confirmed by XRD results (Figure 6). Layered aluminosilicate minerals consist of silicon-oxygen and aluminum-oxygen sheets arranged in specific proportions. Although isomorphous substitution can occur, the bonds between the crystalline layers are relatively weak, making them prone to sliding failure under external forces. Additionally, these minerals have low water absorption between the crystalline layers, with small particle sizes and a compact structure that leads to significant water isolation. This results in the minerals being either impervious or weakly permeable. Consequently, the sliding-zone soil, characterized by high clay content and an abundance of clay minerals, is prone to easy sliding and has poor rainfall infiltration.

From 8 p.m. on 4 September 2019, to 8 a.m. on 5 September 2019, Xiaohe Town in Qiaojia County recorded 190.7 mm of precipitation, reaching heavy rainstorm levels (data from the Geological Disaster Headquarters of Sichuan Province, China). Strong rainfall infiltrated through existing fractures at the trailing edge, where low permeability soil caused rainwater to accumulate in isolated sliding zone spaces, resulting in the formation of supersaturated upper stagnant water. Additionally, continuous rainwater infiltration exacerbated lubrication effects due to clay minerals, particularly layered clay minerals, enhancing the overall instability. The perched groundwater accumulating in the sliding zone creates hydrostatic pressure in fractures, which increases the

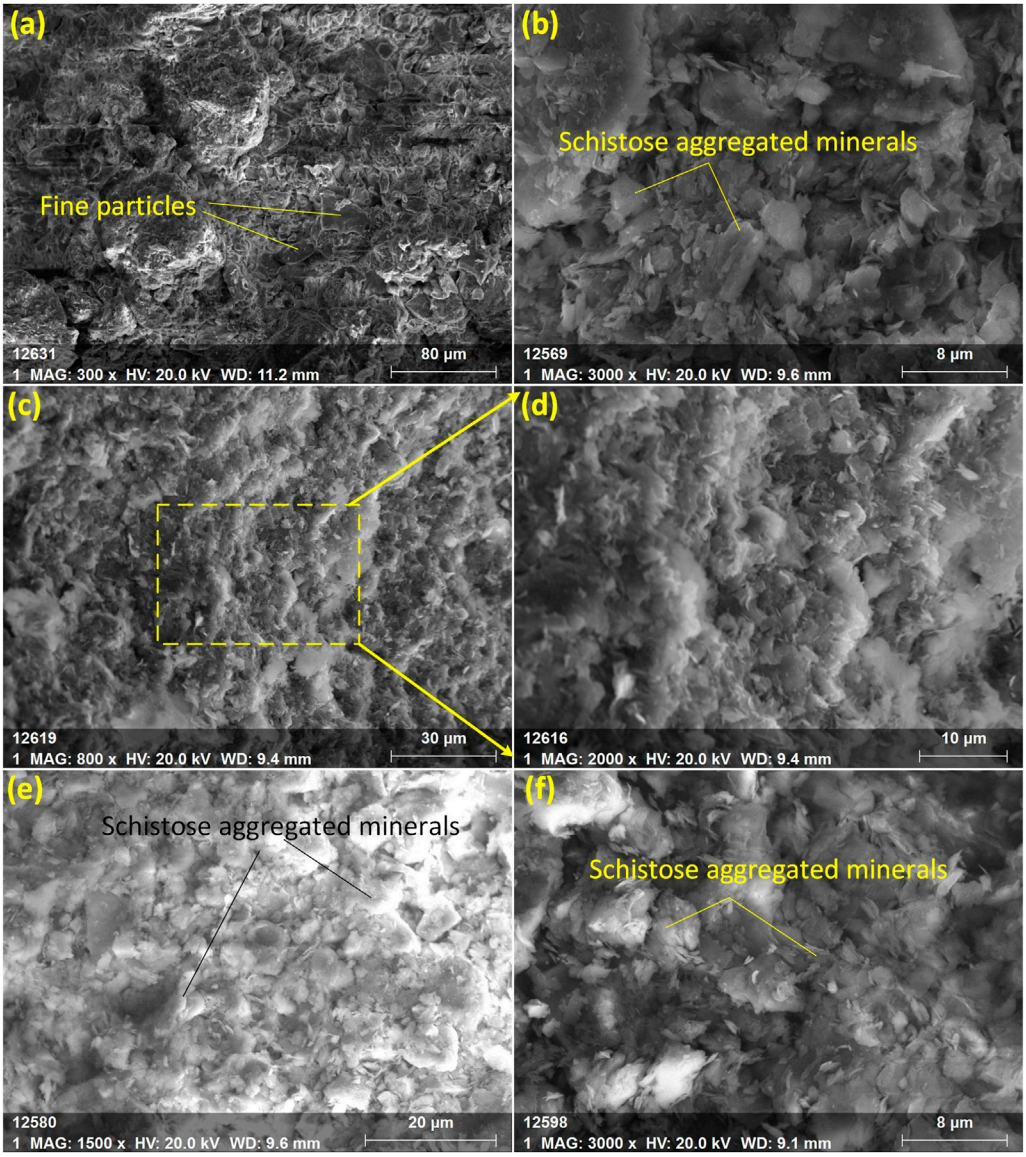

FIGURE 8
Microstructure of the sliding-zone soil from the Lanniqing Landslide. **(A)** is the image at relatively low magnification, showing many fine particles. **(B-F)** are images at higher magnifications in different observation areas, revealing a large amount of schistose aggregated minerals in the slip zone soil. **(D)** is an enlarged view of **(C)**.

sliding force. Simultaneously, the rising pore water pressure within the aquifer further reduces the soil's effective strength, contributing to slope instability. Additionally, continuous rainwater infiltration worsened lubrication effects because the clay minerals, especially layered clay minerals, are easily disrupted. This disruption increases the likelihood that sliding masses will move along the weakened surfaces, particularly during rainfall, thus exacerbating overall instability.

In summary, the landslide is primarily driven by the foundational factors of driving load and excavation related to village road construction, which create a potential sliding surface and induce multi-stage deformation. The sliding surface becomes enriched with clay particles, forming a low-permeability mass high in clay minerals. Rainfall accelerates slope instability, while intrinsic factors such as mineral lubrication and excess pore water pressure from perched groundwater in the sliding zone play crucial roles in triggering the landslide.

It is important to highlight that the Lanniqing landslide is one of many catastrophic landslides in Yunnan province's mountainous watershed, China. These landslides have led to significant casualties among local residents, damage to engineering infrastructure, road destruction, and the loss of forest and agricultural resources. The large deposit masses involved in these landslides create conditions conducive to potential debris flows. This case exemplifies the severe consequences that can arise from the interaction between human engineering activities and natural factors, particularly in alpine

canyon areas shaped by erosion. In areas where people live and require transportation, insufficient economic resources often lead to inadequately supported road slopes, particularly on rural roads. The resulting steep, bare slopes are highly susceptible to disasters, especially under rainfall conditions. To address these issues, the government must regularly inspect and maintain road engineering slopes, improve drainage systems to mitigate the effects of rainfall infiltration, and ensure that slopes remain stable. Additionally, it is crucial to enhance slope monitoring through routine inspections, remote sensing, InSAR, and other technical methods to detect instability signs such as cracks and soil deformation, ensuring effective evacuation of residents before a landslide occurs.

5 Conclusion

(1) Seven different pretreatment methods were applied to soil samples, and particle size was measured using Mastersizer 2000. Comparison of the frequency distribution curves and parameters, such as median and mean particle size, sorting coefficient, skewness, and kurtosis, revealed that both ultrasonic cleaning and $(NaPO_3)_6$ effectively dispersed the particles, with the ultrasonic cleaning demonstrating a more pronounced effect. The use of HCl and the acid removal process led to a reduction in clay content, an increase in silt, and a coarsening of the particle size. In contrast, H_2O_2 had a negligible impact on the results for sliding-zone soil with low organic matter. Based on this comprehensive analysis, pretreatment method C is recommended for more accurate subsequent analysis.

(2) The median and mean particle sizes of the sliding-zone soils were notably smaller compared to those of the undisturbed subsoils, with the former containing a higher proportion of clay particles. Mechanically, the sliding-zone soils generally exhibited higher shear strength and significantly greater cohesion than the undisturbed subsoils. However, the internal friction angle was lower in the sliding-zone soils compared to the undisturbed subsoils. The variations in particle sizes, shear strength, and other indicators, along with observations from the site investigation, reveal that the landslide masses underwent multiple stages of misalignment and sliding before reaching full destabilization.

(3) The driving load and excavation of the village road construction form the foundation of the landslide. Heavy rainfall acts as the triggering factor for slope instability, while the internal causes include mineral lubrication and excess pore water pressure from perched groundwater within the clay-rich sliding zone. The particle size tests, mineral composition analysis, and mechanical strength tests provide essential data on the characteristics and formation-evolution process of the sliding zone. This information supports a deeper understanding of landslide mechanisms and offers new insights into similar mountain slope instability issues related to sliding-zone soil.

(4) To mitigate these risks, it is crucial to enhance the protection of road engineering slopes and improve drainage systems. Regular inspection and maintenance of road slopes in mountainous basins are necessary to maintain slope stability. Additionally, strengthening slope deformation monitoring is essential to ensure timely and effective evacuation of residents before landslides occur.

Data availability statement

The raw data supporting the conclusions of this article will be made available by the authors, without undue reservation.

Author contributions

ZX: Conceptualization, Investigation, Writing–original draft, Writing–review and editing. HY: Investigation, Methodology, Project administration, Writing–review and editing. LL: Visualization, Writing–review and editing.

Funding

The authors declare financial support was received for the research, authorship, and/or publication of this article. This research was financially supported by Yunnan Natural Science Foundation Project (202401AT070119 and 202101AT070138).

Acknowledgments

The authors express their gratitude to ChatGPT-4.0 for its valuable assistance in improving the clarity and expression of this paper. However, we declare that no generative AI techniques were used in the writing process.

Conflict of interest

The authors declare that the research was conducted in the absence of any commercial or financial relationships that could be construed as a potential conflict of interest.

Publisher's note

References

Bai, H. L., Feng, W. K., Li, S. Q., Ye, L. Z., Wu, Z. T., Hu, R., et al. (2022). Flow-slide characteristics and failure mechanism of shallow landslides in granite residual soil under heavy rainfall. *J. Mt. Sci.* 19 (6), 1541–1557. doi:10.1007/s11629-022-7315-8

Callesen, I., Keck, H., and Andersen, J. T. (2018). Particle size distribution in soils and marine sediments by laser diffraction using Malvern Mastersizer 2000-method uncertainty including the effect of hydrogen peroxide pretreatment. *J. soil and sediments* 18, 2500–2510. doi:10.1007/s11368-018-1965-8

Cemiloglu, A., Zhu, L., Mohammednour, A. B., Azarafza, M., Nanehkaran, Y. A., and Ma, M. C. (2023). Landslide susceptibility assessment for Maragheh County, Iran, using the logistic regression algorithm. *Land* 12, 1397. doi:10.3390/land12071397

Chen, J., An, M. K., Long, W., Chen, S., and Teng, Y. B. (2015). Microstructure and mechanism analysis of soil in loose deposit slip zone in Tangjiashan, Yunnan Province. *Eng. Surv.* (1), 7. cnki:sun:gckc.0.2015-01-002. [in Chinese].

Chen, J., Furuichi, M., and Nishiura, D. (2024a). Toward large-scale fine resolution DEM landslide simulations: periodic granular box for efficient modeling of excavatable slope. *Comput. Geotechnics* 165, 105855. doi:10.1016/j.compgeo.2023.105855

Chen, Y. Y., Xu, Z. H., Zhang, Y., and Zha, L. I. (2024b). Study on characteristics of sliding zone soil and occurance mechanism of Qiaojia lanniqing landslide in Zhaotong. *Journal of Natural Hazards* 33 (2), 87–97. doi:10.13577/j.jnd.2024.0209

Chen, Y., Zhang, Y., Wang, L., Wang, S., Tian, D., and Zhang, L. (2022). Influencing factors, deformation mechanism and failure process prediction for reservoir rock landslides: Tanjiahe landslide, three gorges reservoir area. *Front. Earth Sci.* 10, 974301. doi:10.3389/feart.2022.974301

Choi, C. E., and Song, P. (2023). New unsaturated erosion model for landslide: effects of flow particle size and debunking the importance of frictional stress. *Eng. Geol.* 315, 107024. doi:10.1016/j.enggeo.2023.107024

Deng, P., Yi, Q., Zhang, J., Wang, C., Chen, Y., Zhang, T., et al. (2022). Phosphorous partitioning in sediments by particle size distribution in shallow lakes: from its mechanisms and patterns to its ecological implications. *Sci. Total Environ.* 814, 152753. doi:10.1016/j.scitotenv.2021.152753

Dong, J., Zhao, Y., Liu, H., Zhao, J., Zhang, Z., Chi, Q., et al. (2023). Creep characteristics of a strongly weathered argillaceous sandstone sliding zone and the disaster evolution mechanism of the Huaipa landslide, China. *Appl. Sci.* 13 (15), 8579. doi:10.3390/app13158579

Du, Y., He, K., Hu, X., and Ma, H. (2024). Insights into deformation and mechanism of a reactivated landslide occurrence from multi-source data: a case study in Li County, China. *Remote Sens.* 16 (8), 1317. doi:10.3390/rs16081317

Fang, K., Fu, Y., Tang, H., GaoAn, T. P., and Wu, Q. (2024a). Landslide model tests with a miniature 2D principal stress (PS) sensor. *J. Rock Mech. Geotechnical Eng.* doi:10.1016/j.jrmge.2023.12.025

Fang, K., Jia, S., Tang, H., Zhou, R., Kong, Z., Fu, Y., et al.(2024b). Arching effect in slopes under excavation: classification and features.*Eng. Geol.*, 337, 107563. doi:10.1016/j.enggeo.2024.107563

Folk, R. L., and Ward, W. C. (1957). Brazos River bar [Texas]; a study in the significance of grain size parameters. *J. Sediment. Res.* 27 (1), 3–26. doi:10.1306/74D70646-2B21-11D7-8648000102C1865D

Gao, A. S., Guo, R. F., Chai, X. F., and Xu, B. L. (2011). Characteristics of γ meso-scale monomer merging in the catastrophic weather in Xiaohe Town, Zhaotong, China on July 13, 2010. *J. Catastrophology* 26 (2), 6. cnki: sun: zhxu.0.2011-02-020. [in Chinese].

Gidday, B. G., Ayothiraman, R., Ramaiah, B. J., and Ramana, G. V. (2023). Physical and numerical modeling of rainfall triggered shallow landslides in central highlands, Ethiopia. *Bull. Eng. Geol. Environ.* 82 (7), 239. doi:10.1007/s10064-023-03235-y

He, K., Ma, G., Hu, X., and Liu, B. (2021). Failure mechanism and stability analysis of a reactivated landslide occurrence in Yanyuan City, China. *Landslides* 18, 1097–1114. doi:10.1007/s10346-020-01571-8

Huang, R. Q., Pei, X., Fan, X., Zhang, W., Li, S., and Li, B. (2012). The characteristics and failure mechanism of the largest landslide triggered by the Wenchuan earthquake, May 12, 2008, China. *Landslides* 9, 131–142. doi:10.1007/s10346-011-0276-6

Jiang, J. P., Luo, Z. Y., Chen, H., Zhou, D., Sha, D. H., Fang, M. X., et al. (2015). Comparison of two conventional characterization methods of particle diameter. *J. Zhejiang Univ. Eng. Sci. Ed.* 2015 (12), 8. [in Chinese]. doi:10.3785/j.issn.1008-973X.2015.12.012

Jiang, Y., Wang, G., Kamai, T., and McSaveney, M. J. (2016). Effect of particle size and shear speed on frictional instability in sheared granular materials during large shear displacement. *Eng. Geol.* 210, 93–102. doi:10.1016/j.enggeo.2016.06.005

Li, X. (2010). Composition characteristics and genetic significance of slip zone soil. Lanzhou: Lanzhou University. [in Chinese]. doi:10.7666/d.Y1702790

Li, X., Chen, H., Chen, X., Wang, T., Jiang, Y., and Ruan, H. (2024). Experimental study on the stability of noncohesive landslide dams based on seepage effect. *Eng. Geol.* 107708, 107708. doi:10.1016/j.enggeo.2024.107708

Liu, H. L., Han, Z. Y., Li, X. S., and Fang, Y. S. (2012). Influence of pretreatments on grain-size distribution of the red earth in Southern China—a case study on the quaternary red earth profile in Xuancheng, Anhui Province. *Mar. Geol. and Quat. Geol.* 32 (2), 161–167. [in Chinese]. doi:10.3724/SP.J.1140.2012.02161

Ma, Y., Liu, Y., Tian, L., Yang, Y., Long, Y., Lei, M., et al. (2023). Effects of rainfall pattern and soil surface roughness on surface–subsurface hydrological response and particle size distribution of red soil slope. *Catena* 232, 107422. doi:10.1016/j.catena.2023.107422

Mao, Y. M., Li, Y., Teng, F., Arkan, K. S., Azarafza, M., and Zhang, M. S. (2024). Utilizing hybrid machine learning and soft computing techniques for landslide susceptibility mapping in a drainage basin. *Water* 16, 380. doi:10.3390/w16030380

Miao, H., and Wang, G. (2022). Shear rate effect on the residual strength of saturated clayey and granular soils under low-to high-rate continuous shearing. *Eng. Geol.* 308, 106821. doi:10.1016/j.enggeo.2022.106821

Miao, H., and Wang, G. (2023). Prediction of landslide velocity and displacement from groundwater level changes considering the shear rate-dependent friction of sliding zone soil. *Eng. Geol.* 327, 107361. doi:10.1016/j.enggeo.2023.107361

Nanehkaran, Y. A., Chen, B., Cemiloglu, A., Chen, J., Anwar, S., Azarafza, M., et al. (2023). Riverside landslide susceptibility Overview: leveraging artificial neural networks and machine learning in accordance with the United Nations (UN) Sustainable development goals. *Water* 2023, 2707. doi:10.3390/w15152707

Peng, D., Bo, J., Chang, C., Li, X., Duan, Y., and Qi, W. (2023). Study on the geotechnical property changes of loess after seismic landslides—a case study of the Subao Loess landslide in Ningxia, China. *Appl. Sci.* 13 (19), 11023. doi:10.3390/app131911023

Pipatpongsa, T., Fang, K., Leelasukseree, C., Chaiwan, A., and Chanwiset, N. (2024). Reverse toe sliding criteria of laterally confined low wall slope subjected to counterweight fill. *Int. J. Rock Mech. and Min. Sci.* 175, 105683. doi:10.1016/j.ijrmms.2024.105683

Ramaswamy, V., and Rao, P. S. (2006). Grain size analysis of sediments from the northern Andaman Sea: comparisonof laser diffraction and sieve-pipette techniques. *J. Coast. Res.* 22 (4), 1000–1009. doi:10.2112/04-0162.1

Sarbatly, R., Yee, C. P., Fong, T. S., and Krishnaiah, D. (2009). Particle size distribution and purification of red clay for industrial use. *J. Appl. Sci.* 9 (12), 2344–2347. doi:10.3923/jas.2009.2344.2347

Shaanxi North team of Chengdu University of Geology (1978). *Grain size analysis of sedimentary rocks and its application*. Beijing: Geological Publishing House. [in Chinese].

Shen, P., Zhang, L. M., and Zhu, H. (2016). Rainfall infiltration in a landslide soil deposit: importance of inverse particle segregation. *Eng. Geol.* 205, 116–132. doi:10.1016/j.enggeo.2015.09.008

Su, X., Wu, W., Tang, H., Huang, L., Xia, D., and Lu, S. (2023). Physicochemical effect on soil in sliding zone of reservoir landslides. *Eng. Geol.* 324, 107249. doi:10.1016/j.enggeo.2023.107249

Wang, C., Yi, Q., Wan, K., and Zhang, J. (2023). Partitioning pattern of metals onto sediment particles in shallow lakes: an exponential decrease with increased particle size and its environmental implications. *J. Soils Sediments* 23 (1), 483–495. doi:10.1007/s11368-022-03389-4

Wang, J. J., Zhao, D., Liang, Y., and Wen, H. B. (2013). Angle of repose of landslide debris deposits induced by 2008 Sichuan Earthquake. *Eng. Geol.* 156, 103–110. doi:10.1016/j.enggeo.2013.01.021

Wang, L., Li, X. A., Hong, B., Zhao, N., and Li, L. C. (2018). Experimental study on the effect of pretreating method on grain size distribution pattern of Malan Loess. *Earth Environ.* 46 (2), 210–217. [in Chinese]. doi:10.3724/SP.J.1140.2012.02161

Wang, Q., Tang, H., An, P., Fang, K., Zhang, J., Miao, M., et al. (2024). Insight into the permeability and microstructure evolution mechanism of the sliding zone soil: a case study from the Huangtupo landslide, Three Gorges Reservoir, China. *J. Earth Sci.* 35 (3), 941–954. doi:10.1007/s12583-023-1828-0

Wang, Y., Li, K., Li, J., and Tang, S. (2021). Influence of soil particle size on the engineering properties and microstructure of a red clay. *Appl. Sci.* 11 (22), 10887. doi:10.3390/app112210887

Wei, H., Liu, E., Wei, X., He, C., Chen, L., and Li, Q. (2024). Thermo-hydro-mechanical (THM) analysis of rock-ice avalanches: considering the effects of particle breakage in the sliding zone. *Cold Regions Sci. Technol.* 219, 104123. doi:10.1016/j.coldregions.2024.104123

Wolter, A., Gasston, C., Morgenstern, R., Farr, J., Rosser, B., Massey, C., et al. (2022). The Hapuku Rock Avalanche: breaching and evolution of the landslide dam and outflow channel revealed using high spatiotemporal resolution datasets. *Front. Earth Sci.* 10, 938068. doi:10.3389/feart.2022.938068

Yaser, A. N., Zhu, L., Jin, C., Chen, J., Anwar, S., Azarafza, M., et al. (2023). Comparative analysis for slope stability by using machine learning methods. *Appl. Sci.* 8. doi:10.3390/app13031555

Yin, Z. Q., Wei, G., and Tang, Y. G. (2012). Multi-component distribution characteristics of soil and sediments in landslide zone (surface). *J. Eng. Geol.*, 20(6), 998–1006. doi:10.3969/j.issn.1004-9665.2012.06.012[in Chinese]

Zha, L. L., Xu, Z. H., and Zhang, Y. (2022). Effects of different pretreatment methods on grain size characteristics of sediments from landslide-dammed lake based on Mastersizer 2000. *Quat. Res.* [in Chinese]. doi:10.11928/j.issn.1001-7410.2022.06.14

Zhang, D., Li, L. X., Hu, X. L., Niu, L. F., Wang, B., and Wang, Q. (2021). Influence of long-term static water soaking on physico-chemical-mechanical properties of slip-belt soil in the Three Gorges Reservoir area. *Geol. Sci. Technol. Inf.* 040 (005), 0120211200269970. [in Chinese]. doi:10.19509/j.cnki.dzkq.2021.0041

Zhang, L., Zhong, Q., Yang, M., Peng, M., Liu, J., Mei, S., et al. (2023). Centrifugal model tests and numerical modeling on overtopping-induced breach processes of landslide dams. *Front. Earth Sci.* 10, 1062981. doi:10.3389/feart.2022.1062981

Zhang, Y., Zhang, W., Wang, L., Xiao, T., Meng, X., and Zhang, Z. (2024). Mechanism of the high-speed and long-run-out landslide considering the evolution of the frictional heat in the sliding zone. *Nat. Hazards* 120 (4), 3299–3317. doi:10.1007/s11069-023-06334-x

Zhang, H., H., Liu, Y., Dang, X., Meng, Z., Li, S., and Gao, Y. (2024). Particle size characterization and sources of sediments in the Uzhumqin sand dunes. *J. Mt. Sci.* 21 (8), 2631–2645. doi:10.1007/s11629-023-8577-5

Zhao, H. F., Zhang, L. M., Xu, Y., and Chang, D. S. (2013). Variability of geotechnical properties of a fresh landslide soil deposit. *Eng. Geol.* 166, 1–10. doi:10.1016/j.enggeo.2013.08.006

Zhao, L., Tian, W., Liu, K., Yang, B., Guo, D., and Lian, B. (2024). An empirical relationship of permeability coefficient for soil with wide range in particle size. *J. Soils Sediments* 24, 2926–2937. doi:10.1007/s11368-024-03743-8

Zhao, Z. S., and Xu, W. Z. (2013). Analysis on the causes and prevention measures of Lufanggou debris flow disaster in Xiaohe Town, Qiaojia County, Yunnan Province. *Value Eng.* 32 (4), 291–293. [in Chinese]. doi:10.14018/j.cnki.cn13-1085/n.2013.04.008

Zhou, Y., Shi, Z., Zhang, Q., Liu, W., Peng, M., and Wu, C. (2019). 3D DEM investigation on the morphology and structure of landslide dams formed by dry granular flows. *Eng. Geol.* 258, 105151. doi:10.1016/j.enggeo.2019.105151

Zhu, Q., Qi, X., Cheng, X., and Zhou, Z. (2024). Estimating sediment transport capacity on sloping farmland on the Loess Plateau considering soil particle size characteristics. *Geoderma* 446, 116906. doi:10.1016/j.geoderma.2024.116906

Zhuo, L., Hu, Y. F., Xiao, M. L., Luo, Y., Liu, H. Z., Xie, H. Q., et al. (2023). Experimental and statistical study on the formation characteristics and discrimination criteria of river blockages caused by landslides. *Appl. Sci.* 13 (21), 12003. doi:10.3390/app132112003